Effects of particle shape mixture on strength and structure of sheared granular materials

Theechalit Binaree,[1,*] Itthichai Preechawuttipong,[1,†] and Emilien Azéma[2,‡]
[1]*Department of Mechanical Engineering, Faculty of Engineering, Chiang Mai University, 239 Huay Kaew Rd., Chiang Mai 50200, Thailand*
[2]*LMGC, Université Montpellier, CNRS, Montpellier, France*

(Received 7 February 2019; published 15 July 2019)

Using bi-dimensional discrete element simulations, the shear strength and microstructure of granular mixtures composed of particles of different shapes are systematically analyzed as a function of the proportion of grains of a given number of sides and the combination of different shapes (species) in one sample. We varied the angularity of the particles by varying the number of sides of the polygons from 3 (triangles) up to 20 (icosagons) and disks. The samples analyzed were built keeping in mind the following cases: (1) increase of angularity and species starting from disks; (2) decrease of angularity and increase of species starting from triangles; (3) random angularity and increase of species starting from disks and from polygons. The results show that the shear strength vary monotonically with increasing numbers of species (it may increase or decrease), even in the random mixtures (case 3). At the micro-scale, the variation in shear strength as a function of the number of species is due to different mechanisms depending on the cases analyzed. It may result from the increase of both the geometrical and force anisotropies, from only a decrease of frictional anisotropy, or from compensation mechanisms involving geometrical and force anisotropies.

DOI: 10.1103/PhysRevE.100.012904

I. INTRODUCTION

Granular systems in nature and in industry are rarely composed of grains having the same size (monodisperse) or the same shape. They are rather mixtures of particles of varying sizes, shapes, density, or mechanical properties [1–8]. For instance, concrete aggregates present a very wide grain size distribution (GSD) that strongly modifies its performance and workability [9–12]. This is also true in drug substances, for which physicochemical and biopharmaceutical properties depend on the particle size of there constitute [13].

Samples containing different particles sizes (polydisperse) have been extensively analyzed [6,14–20], showing some counterintuitive results such as the independence of the macroscopic friction with respect to the grain size span [21,22], the shape of the GSD [23,24], and stiffness and Poisson's ratio of the particles [25,26].

At the same time, an increasing number of laboratory tests and numerical studies have shown the role of grain shape on the packing properties and mechanical behavior of granular materials [27–44]. Across these studies, we can notice that there is no a single parameter for describing grain shape. Several parameters for angularity/roundedness, elongation, or platy-ness have been used to characterize the shape of the particles. However, a systematic result is that the shear strength varies non-linearly with packing fraction as particle shape changes from spherical to very angular forms [45,46], with non-convexity [47,48], and with anisometry (elongation/platy-ness) [49,50].

Granular materials having two distinctive particle shapes, also known as binary mixtures, are of special interest in recent investigations [51–54]. It was shown that particle segregation can be observed when varying either grain size or shape [55–57], yet the strength properties are nearly independent of the degree of homogeneity of the packing [58].

In spite of this important progress in the analysis of grain geometry and the corresponding mechanical behavior, the effect of multiple particle shapes in a sample is still a subject to explore. However, it is not trivial to build and analyze systems composed of very different particle shapes. Segregation should be carefully controlled and larger packings have to be considered in order to avoid effects related with local particle ordering and clustering.

In this paper, we propose to explore the effects of particle shape polydispersity on the mechanical behavior of sheared granular packings, using contact dynamic simulations. We use regular polygonal particles since their shape can be described by a single shape parameter, i.e., their angularity defined from the number of sides. Packings composed of several angular particles (from 1 to 10 species) are studied in the quasi-static shear state. We analyze the strength and packing fraction at the macroscopic scale and the connectivity and anisotropy of the contact and force networks at the microscopic scale, both as a function of the number and shape of species.

In the following, we present the numerical method, the packing construction and the parameters of the study (Sec. II). Then, in Sec. III, the dependence of the macroscopic behavior with respect with particle shape polydispersity is discussed. A microstructural description is given in terms of particle connectivity, stress transmission, and anisotropies of the fabric and force network in Sec. IV. The results are summarized and discussed in a concluding section.

*theechalit_b@cmu.ac.th
†itthichai.p@cmu.ac.th
‡emilien.azema@umontpellier.fr

TABLE I. Numerical samples. The number of species N_s in each numerical series S1 to S4. The numbers in brackets refers to the number of sides of the polygons of each species i with $i \in [1, N_s]$.

N_s	S1	S2	S3	S4
1	{disk}	{3}	{disk}	{7}
2	{disk,20}	{3,4}	{disk,3}	{7,5}
3	{disk,20,15}	{3,4,5}	{disk,3,20}	{7,5,15}
4	{disk,20,15,10}	{3,4,5,6}	{disk,3,20,4}	{7,5,15,10}
5	{disk,20,15,10,8}	{3,4,5,6,7}	{disk,3,20,4,15}	{7,5,15,10,4}
6	{disk,20,15,10,8,7}	{3,4,5,6,7,8}	{disk,3,20,4,15,5}	{7,5,15,10,4,disk}
7	{disk,20,15,10,8,7,6}	{3,4,5,6,7,8,10}	{disk,3,20,4,15,5,10}	{7,5,15,10,4,disk,8}
8	{disk,20,15,10,8,7,6,5}	{3,4,5,6,7,8,10,15}	{disk,3,20,4,15,5,10,6}	{7,5,15,10,4,disk,8,6}
9	{disk,20,15,10,8,7,6,5,4}	{3,4,5,6,7,8,10,15,20}	{disk,3,20,4,15,5,10,6,8}	{7,5,15,10,4,disk,8,6,20}
10	{disk,20,15,10,8,7,6,5,4,3}	{3,4,5,6,7,8,10,15,20,disk}	{disk,3,20,4,15,5,10,6,8,7}	{7,5,15,10,4,disk,8,6,20,3}

II. NUMERICAL PROCEDURES, PACKING CONSTRUCTION, AND BIAXIAL TEST

We use the Non-Smooth Contact Dynamics (NSCD) method originally developed by Moreau and Jean [59,60]. This method is a discrete element approach for the simulation of non-smooth granular dynamics with contact laws expressing non-penetrability of the particles and dry friction between particles. It is unconditionally stable and well suited to the simulation of large packing composed of frictional particle of any shapes. For specific implementation of the method, see [60] and [45] for the handling of polygonal particles. We have used the simulation platform known as LMGC90 developed in Montpellier and capable of modeling a collection of deformable or undeformable particles of various shapes (spherical, polyhedral, polygonal, non-convex) by different algorithms [60–62].

In general, a granular mixture is defined by, at least, three parameters: (1) the number of species N_s, (2) a set $\{\alpha_i\}_{i\in[1,N_s]}$ describing the properties of each species i, and (3) the proportion κ_i of each specie. For the sake of simplicity, and in order to reduce the number of parameters, we will assume a uniform distribution by particle number, so that $\kappa_i = 1/N_s$. The number of particles of each species is thus simply given by N_p/N_s, where N_p is the total number of particles. We consider regular polygonal particles with the number of sides $n_s \in [3, 4, 5, 6, 7, 8, 10, 15, 20]$, and circular particles. So, α_i which will refer as the angularity of the specie i is simply given by $2\pi/n_s^i$, where n_s^i is the number of side of the specie i. Note that the shear behavior of a packing composed of polygons of $n_s > 20$ is nearly identical to those of a packing of disks [45]. In the following the number of species N_s is varied from 1 to 10, and four different packings series are considered: ($S1$) increase of angularity with N_s, ($S2$) decrease of angularity with N_s, and ($S3$) and ($S4$) random angularity with N_s; see Table I for a better description of the composition of each packings. A total of 37 packings were built. Note that for $N_s = 10$ all series are identical.

Each packing is composed of a total of $N_p = 10\,000$ particles, randomly placed into a rectangular box by means of simple geometrical rules in order to build a dense system [63]. A small size polydispersity is considered by taking d (the diameter of circumscribing circle of the particle) in the range $[d_{\min}, d_{\max}]$ with $d_{\max} = 1.25 d_{\min}$ with a uniform distribution in particle area fractions. Then, all packings are isotropically compacted by applying a constant compressive stress σ_0 on each wall. During this process, the gravity, the friction coefficients between particles and friction coefficient between particles and walls are set to zero. This procedure leads to obtain a dense system close to the so-called random close packing state. Zooms of the packings are shown in Fig. 1, for different values of N_s in S1, S2, S3, and S4, at the end of isotropic compaction.

Dense samples obtained at the end of the isotropic compression are then subjected to bi-axial shearing by imposing a vertical compression at a constant velocity v_y of the top wall and a constant confining stress σ_0 acting on the lateral walls. For the bi-axial shearing, the friction coefficient between particles is set to 0.4 whereas wall friction is maintained to 0.0. We are interested in the quasi-static (rate-independent) behavior which can be quantified through the inertial number

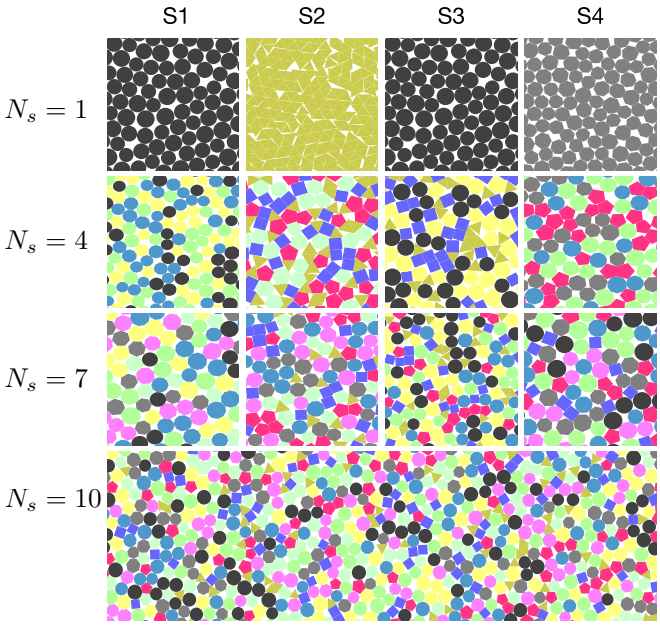

FIG. 1. Closeup views of some of the samples at the end of the isotropic compression. Disks are shown in black, triangles in dark yellow, squares in blue, pentagons in red, hexagons in light green, heptagons in gray, octagons in light pink, dodecagons in light blue, pentadecagons in mint green, and icosagons in yellow.

$I = \dot{\varepsilon}\sqrt{m/\sigma_0}$ [64], where $\dot{\varepsilon} = \dot{y}/y$ is the strain rate and m is the average mass of a particle. To ensure that all shear tests remain quasi-static, I was fixed to 10^{-4}.

III. MECHANICAL BEHAVIOR AT MACROSCOPIC SCALE

For quasi-static shearing, the shear strength of dry granular materials is classically quantified via the macroscopic friction angle φ defined by

$$\sin\varphi = \frac{q}{p}, \tag{1}$$

where $q = (\sigma_1 - \sigma_2)/2$ and $p = (\sigma_1 + \sigma_2)/2$ with σ_1 and σ_2 the principal stresses (eigenvalues) of the stress tensor. In granular assemblies, the stress tensor is defined as the sum of $\boldsymbol{M}^{\xi}$, the "tensor moment" of each particle ξ in a volume (area in 2D) V, by [65–67]

$$\boldsymbol{\sigma} = \frac{1}{V}\sum_{\xi\in V}\boldsymbol{M}^{\xi}, \tag{2}$$

where $\boldsymbol{M}^{\xi}_{kj} = \sum_{c\in\xi} f^c_k r^c_j$ with f^c_k is the k component of the force exerted on particle ξ at the contact c, r^c_j is the j component of the position vector of the same contact c, and the sum is done over all contact neighbors of particle ξ (noted by $c \in \xi$). Let us define also the deviatoric strain $\varepsilon_q = \varepsilon_1 - \varepsilon_2$, where $\varepsilon_1 = \Delta H/H_0$ and $\varepsilon_2 = \Delta L/L_0$ with H_0 and L_0 the initial height and width of the simulation box,

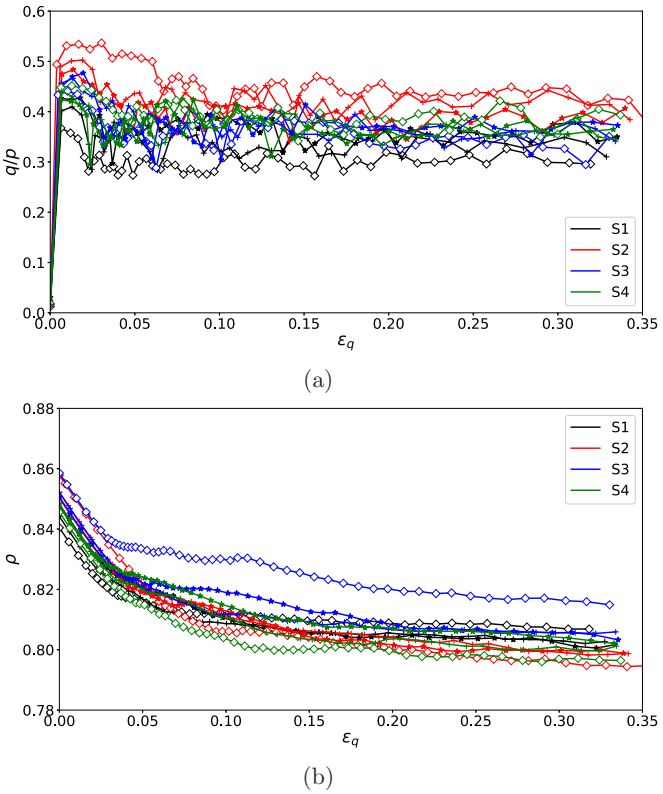

FIG. 2. Evolution of the stress ratio q/p (a) and the packing fraction ρ (b) as functions of the deviatoric strain ε_q in each series for $N_s = 4$ ($\diamond$), $N_s = 7$ ($+$), and $N_s = 9$ ($\star$) in $S1$, $S2$, $S3$, and $S4$.

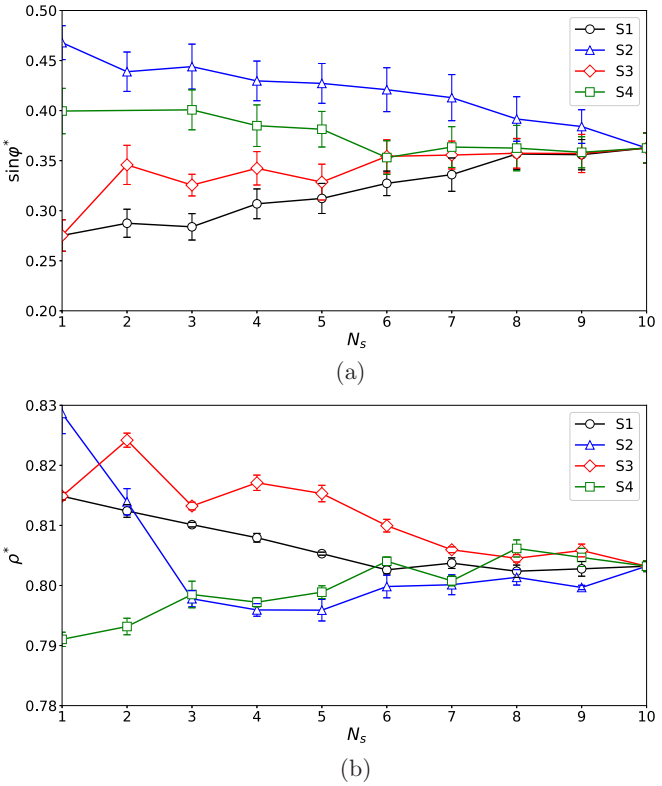

FIG. 3. Macroscopic shear strength $\sin\varphi^*$ and packing fraction ρ^*, averaged in the residual state, as a function of the number of species N_s, for $S1$ (back circle), $S2$ (blue triangle), $S3$ (red diamond), and $S4$ (green square).

and $\Delta H = H_0 - H$ and $\Delta L = L_0 - L$ are the corresponding cumulative displacements.

The evolution of q/p as a function of the deviatoric strain ε_q is shown in Fig. 2(a) for values of $N_s = 4, 7, 9$ in $S1$, $S2$, $S3$, and $S4$. As expected, we obtain an increase of shear strength up to a peak (because of the high initial packing fraction and perfect rigidity of the particles), followed by a slight decrease and reaching a stress plateau corresponding to the "residual state" in soil mechanics [68].

The evolution of packing fraction $\rho = V_p/V$ (where V_p is the volume occupied by the particles) is shown in Fig. 2(b) as a function of ε_q for $N_s = 4, 7, 9$ in $S1$, $S2$, $S3$, and $S4$. Again, a general observation is that ρ quickly declines, i.e., the packings dilate, from ρ_0 (its value at the initial state) to a nearly constant value in the residual state for $\varepsilon_q \simeq 0.20$. In the following, all presented quantities correspond to averaged values in the residual state, with the corresponding errors bars displaying the standard deviation of the data.

Figure 3 shows the macroscopic friction angle $\sin\varphi^*$ and the solid fraction ρ^*, both defined from the averaged values of q/p and ρ, respectively, in the residual state and as a function of N_s for all series. We see that the shear strength increases in $S1$ and $S3$ from $\simeq 0.28$ to $\simeq 0.36$ whereas it declines from $\simeq 0.48$ to $\simeq 0.36$ for $S2$ and from $\simeq 0.40$ to $\simeq 0.36$ for $S4$. Previous results have shown that, in packings composed of identical angular shapes, the shear strength increases first with angularity and saturates to a limit value that is independent of particle angularity [45,46]. The monotonous variation of

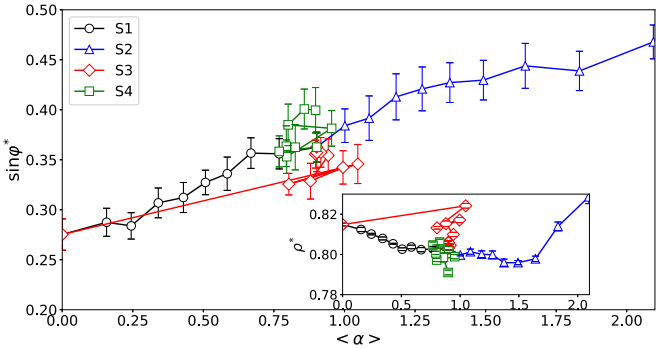

FIG. 4. Macroscopic shear strength $\sin\varphi^*$ and packing fraction ρ^* (inset), averaged in the residual state, as a function of the mean angularity $\langle\alpha\rangle$ for all series.

$\sin\varphi^*$ that we observe in $S1$ and $S2$ can be understood since we add particles with more and more (or less and less) sides. In contrast, this finding is a rather counterintuitive finding for $S3$ and $S4$ as one could rather expect a non-monotonous and marked variation.

In contrast, we note that ρ^* declines with N_s for $S1$ and $S3$ from ∼0.81 to ∼0.80, while it increases with N_s for $S4$ from ∼0.79 to ∼0.80, and it declines again from ∼0.83 to ∼0.80 before to remain independent of N_s for $S2$.

The macroscopic friction $\sin\varphi^*$ and the packing fraction ρ^* can be also plotted as a function of the mean angularity $\langle\alpha\rangle$ of each packing; see Fig. 4. A general observation is that the macroscopic friction increases with the mean angularity. A continuous variation of both, $\sin\varphi^*$ and ρ^* with $\langle\alpha\rangle$, is observed between $S1$ and $S2$. This was expected since these two series are "symmetric" from packings composed of ten species. Unfortunately, no collapse of the data is observed for random mixtures and, furthermore, significant differences in values of $\sin\varphi^*$ and ρ^* are observed at identical values of the mean angularity. This last observation suggests that the nature of the mixture had deep effects on the granular microstructure as we will see below.

IV. PARTICLE SCALE DESCRIPTION

In this section, we present a quantitative description of the microstructural properties of our mixtures of angular particles with the aim of identifying the origins of the shear strength. We focus particularly on particle connectivity, the role of each species in stress transmission as well as on the force/fabric anisotropies of the contact network.

A. Particle connectivity

Figure 5 shows a snapshot of the contact network in the residual state for the series $S2$ and for $N_s = \{1, 4, 7, 10\}$. Visual inspection reveals that the contact network topology strongly varies with particle shapes. Here, for $S2$, we observe a rapid decrease of density where packings composed of only triangles seem to be well connected with small voids, whereas larger voids are observed for packings composed by a larger number of different species. Quantitatively, the simplest statistical descriptors to characterize the connectivity of the contact network are the proportion K_f of floating particles,

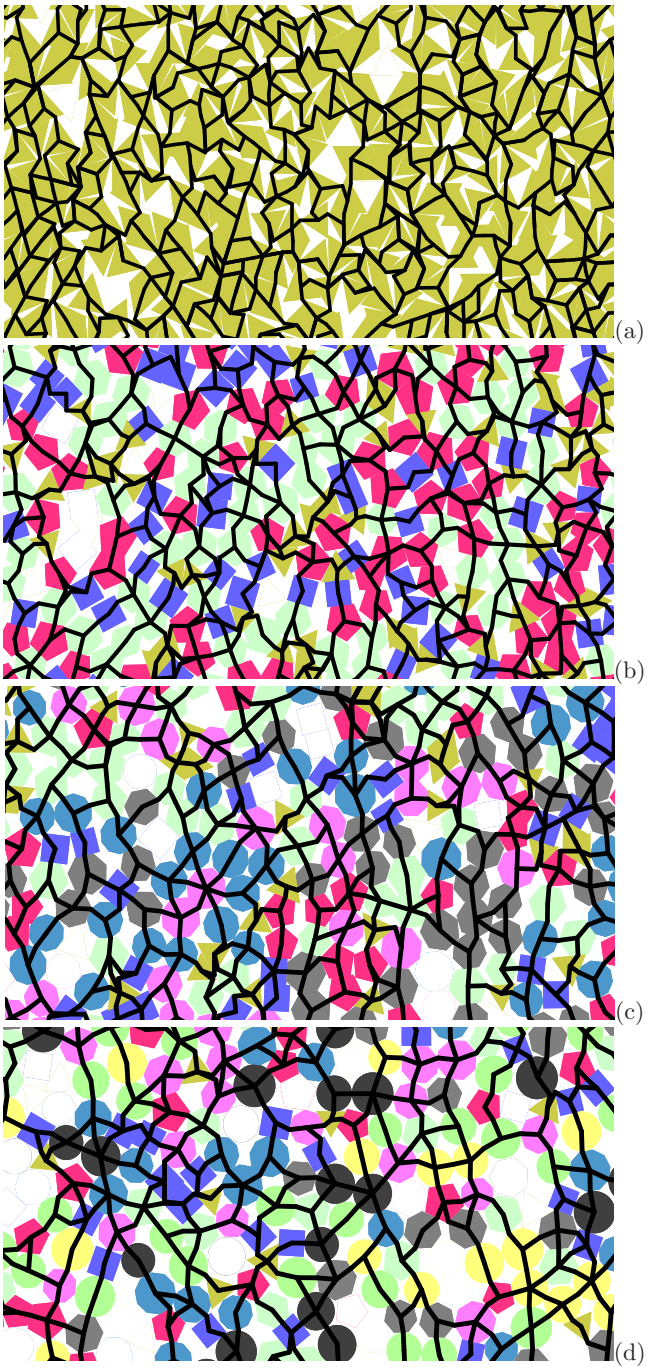

FIG. 5. Contact networks in $S2$ for $N_s = 1$ (a), $N_s = 4$ (b), $N_s = 7$ (c), and $N_s = 10$ (d) in the residual state. Rattlers, i.e., particles with no contact, are in white with color borders. Black lines join the centers of mass of the grains to the contact points. Colors are the same as in Fig. 1.

i.e., particles carrying no load, often referred to as the rattlers, and the coordination number Z (average number of force-bearing contacts per non-floating particle).

Figure 6 shows K_f and Z as functions of N_s for each series. We see that K_f and Z are nearly independent of N_s in $S1$ and $S4$ with values around 0.15 and 3.2, respectively. Indeed, in these two cases the first particles who are mixed can be considered as rounded particles with a similar steric exclusion

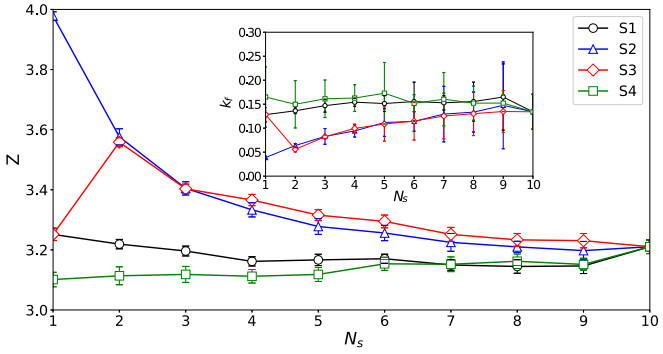

FIG. 6. Coordination number Z as a function of N_s for each series. The inset shows the proportion K_f of floating particles as a function of N_s for each series.

angle among the neighboring particles [69]. In contrast K_f increases for $N_s > 1$ from ∼0.05 to ∼0.15 for $S2$ and $S3$, whereas Z declines from ∼3.6 to ∼3.1. In these last two cases, we note that the first particles that are mixed are the most angular. They are as well those with the most sharped corners and, therefore, the ones more likely to form contacts that would be impossible when having more rounded particles. It is interesting to note that Z do not follows the evolution of $\sin\varphi^*$, showing that the best connected systems are not necessarily those with the higher shear strength.

We must mind the fact that in a system composed of polygons, two families of contacts co-exist: side-side (ss) and side-vertex (sv) contacts. In Fig. 7, we plot Z_{ss} and Z_{sv}, the

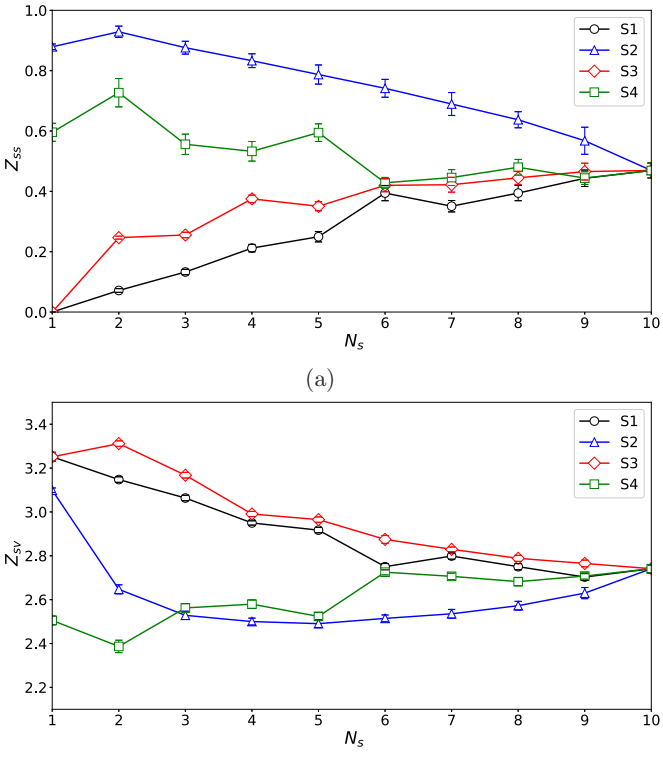

FIG. 7. Coordination number Z_{sv} and Z_{ss} as a function of N_s for each series.

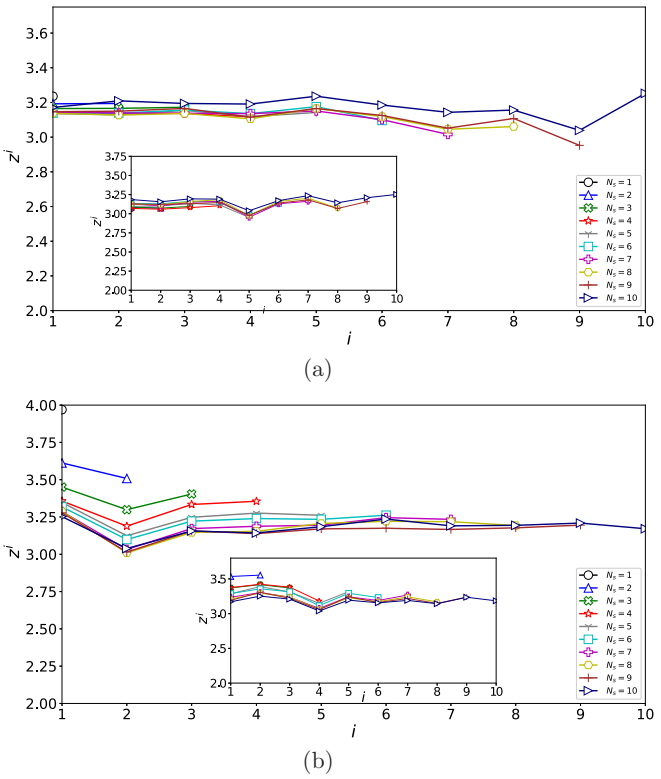

FIG. 8. Average coordination number z^i for each species i (with $i \in [1, N_s]$) in (a) $S1$ and $S4$ (inset), and (b) $S2$ and $S3$ (inset).

mean number of side-side and side-vertex contacts per grain, as a function of N_s, for all series. Note that, by construction $Z = Z_{ss} + Z_{sv}$. We see that the independence of Z with N_s, i.e., $S1$ and $S4$ cases, results from the opposite variations of Z_{sv} and Z_{ss}. The decrease of Z with N_s, i.e., $S2$ and $S3$ cases, is due to the decrease of Z_{ss} in $S2$ and the decrease of Z_{sv} in $S3$. Furthermore, we note that Z_{ss} increases with N_s both for $S1$ and $S3$, whereas it declines with N_s both for $S2$ and $S4$. In other words, Z_{ss} follows a similar trend to that of $\sin\varphi$, confirming previous observations [35,38,45,46,49,70] on the major role of ss contacts in the build-up of the shear strength.

B. Role of each particles species in stress transmission

In order to get further insight into the geometrical properties of the contact network, it is useful to consider the connectivity of each species i with $i \in [1, N_s]$. We define z^i the mean coordination number of the specie i, such $Z = \langle z^i \rangle$. Figure 8 shows the variations of z^i as a function of i in $S1$, $S4$ (a) and $S2$, $S3$ (b). A counterintuitive observation is that z^i is independent of both the number and nature of the species in $S1$ and $S4$, and the number of species in $S2$ and $S3$. In this last case the increase of N_s leads to a decrease of z^i. This means as well that, for a given mixture, each species have in average the same number of contacts.

Along with the same line as above, the stress tensor can be partitioned as a sum of various tensors by grouping each particles according to their species:

$$\boldsymbol{\sigma} = \sum_{i\in[1,N_s]} \boldsymbol{\sigma}^i, \tag{3}$$

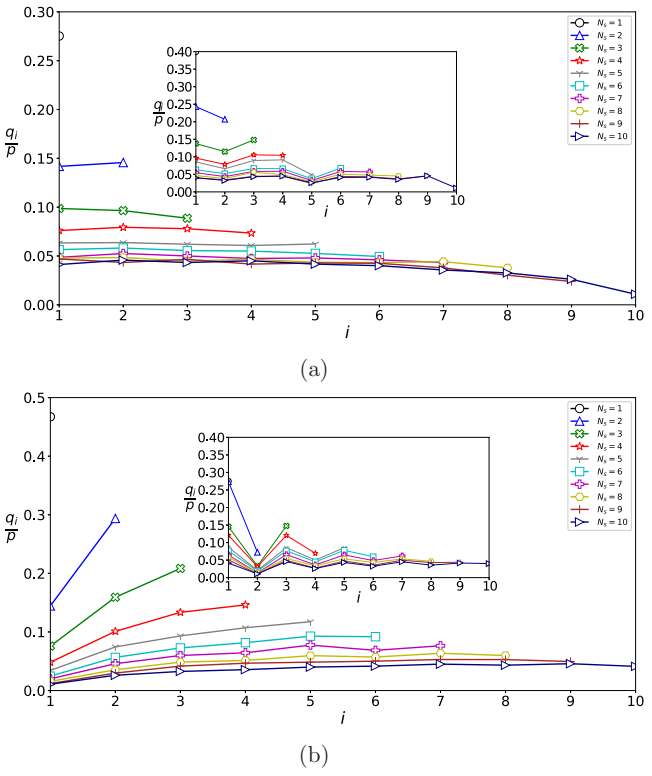

FIG. 9. Partial shear strength q^i/p for $i \in [1, N_s]$ for each species i (with $i \in [1, N_s]$) in (a) $S1$ and $S4$ (inset), and (b) $S2$ and $S3$ (inset).

where $\boldsymbol{\sigma}^i$ are obtained from the expression of the stress tensor Eq. (2) by restricting the summation to particles belonging to the same species. The corresponding partial stress deviators q_i are then calculated and normalized by the mean pressure p. The macroscopic friction angle can be thus rewritten as follows:

$$\sin\varphi^* = \sum_{i\in[1,N_s]} \frac{q^i}{p}. \tag{4}$$

Figure 9 shows the partial shear strength q^i/p for each species i in each series. We see that, in $S1$ and $S4$, q^i/p is nearly constant with i but declines from $\simeq 0.15$ to $\simeq 0.05$ as N_s increases from 1 to 5. Interestingly, beyond $N_s = 5$, q^i/p stays independent of N_s. In a similar vein, in $S2$ we observe that q^i/p increases with i but declines and saturates as N_s increases. As observed above, it tends to be also independent of N_s from five species. In $S3$, we see that q^i/p increases and declines as i increases while $N_s < 5$, and remains independent beyond $N_s = 5$. A general feature that emerge from these observations is that the shape polydispersity plays a minor role at high species polydispersity (typically for more than five species). An other interesting remark is that less angular particles support larger stresses than more angular particles, while in average all particles have the same number of contacts.

C. Contact/force anisotropies

Figure 10 shows several maps of normal forces for mixtures composed of four species, i.e., $N_s = 4$. The normal forces are represented with a line joining the particle center and its thickness is proportional to force intensity. We observe that long force chains are preferentially oriented along the compression direction, i.e., at 90 degrees. But, they appear to have more tortuous shape in $S2$ and $S4$ than in $S1$. We also observe a pronounced arching effect in $S3$. Such pictures reveal the anisotropic character of the contact and force networks.

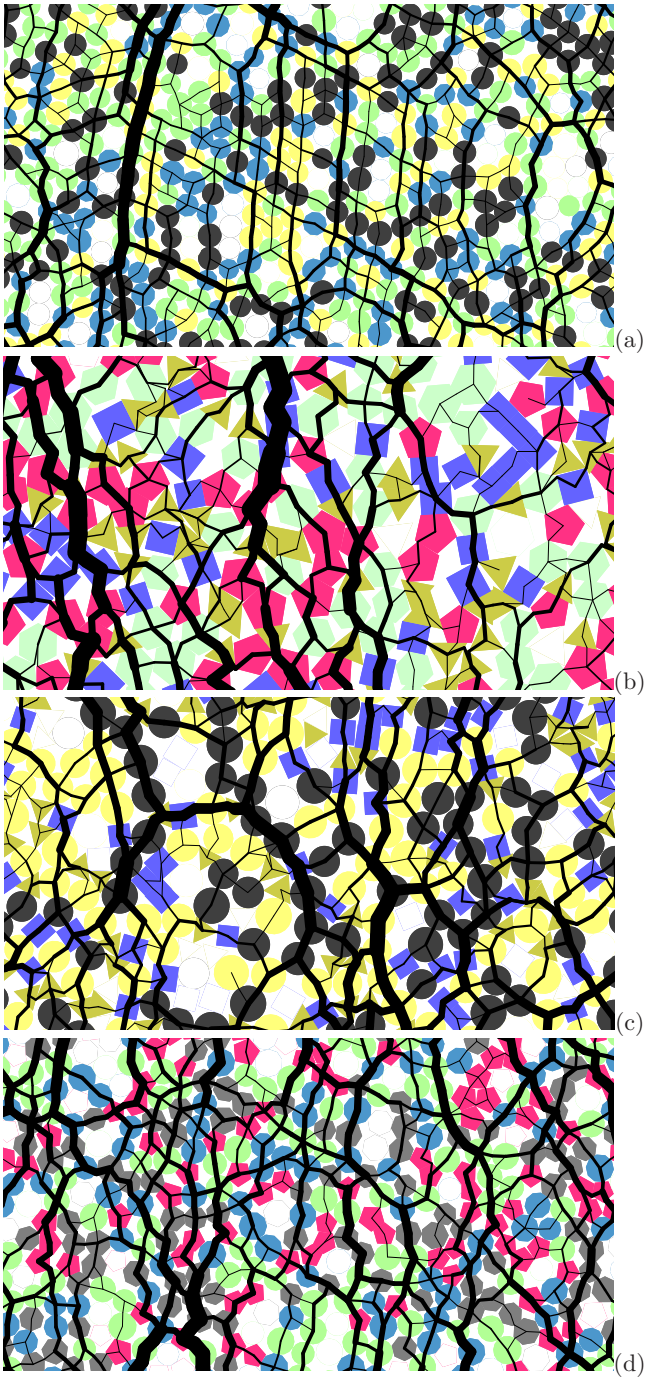

FIG. 10. Snapshots of the force network for $N_s = 4$ in $S1$ (a), $S2$ (b), $S3$ (c), and $S4$ (d) in the residual state. Rattlers, i.e., particles with no contacts, are shown in white with colored borders. Line thickness is proportional to the contact force. Colors of the particles are the same as in Fig. 1.

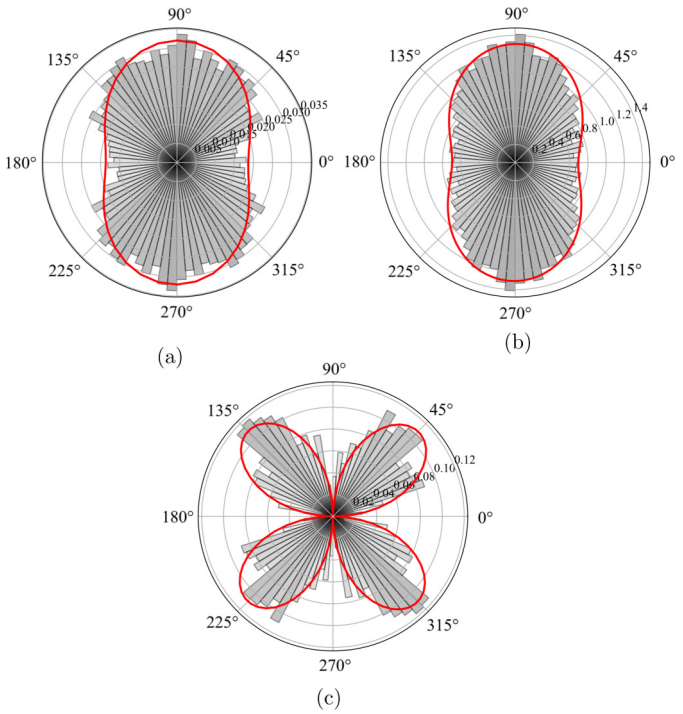

FIG. 11. Probability density functions $P(\theta)$ (a), $\langle f_n\rangle(\theta)$ (b), and $\langle f_t\rangle(\theta)$ (c) (symbols) with the truncated Fourier approximations (red lines) for $S3$ and $N_s = 4$.

As shown in a number of previous studies (see, for example, [24,45–50,71]), the most relevant way to quantify the anisotropy of the fabric and force network is done by computing the probability distribution function $P(\boldsymbol{n})$ of contact orientation $\boldsymbol{n}$, and the average contact force $\langle \boldsymbol{f}\rangle(\boldsymbol{n})$ as a function of $\boldsymbol{n}$. In two dimension, the normal vector is simply defined by an angle θ, and the average contact force can be split according to its normal and tangential contributions. So that, the probability density $P(\theta)$ of contact orientation θ and the angular averages of the normal and tangential force component, $\langle f_n\rangle(\theta)$ and $\langle f_t\rangle(\theta)$, respectively, provide a complete description of the fabric and force anisotropies of a granular material.

In continuous quasi-static shearing, these functions tend to take a simple shape, well approximated by truncated Fourier expansions [24,45–50,71]:

$$\begin{cases} P(\theta) &= \frac{1}{2\pi}\{1 + a_c \cos 2(\theta - \theta_c)\}(a) \\ \langle f_n\rangle(\theta) &= \langle f_n\rangle\{1 + a_{fn} \cos 2(\theta - \theta_{fn})\}(b) \\ \langle f_t\rangle(\theta) &= \langle f_n\rangle a_{ft} \sin 2(\theta - \theta_{ft})(c), \end{cases} \quad (5)$$

where $\langle f_n\rangle$ is the mean normal force, a_c is the contact orientation anisotropy, a_{fn} is the normal force anisotropy, and a_{ft} is the frictional force anisotropy. The main orientations for each angular distribution, θ_c, θ_{fn}, and θ_{ft}, nearly match the principal stress direction $\theta_\sigma = \pi/2$ in a bi-axial simulation, as illustrated in Fig. 11 for $N_s = 4$ in $S3$. We see also in this figure that Eq. (5) provides an acceptable approximation of the angular distributions.

Assuming low span in the particle size distribution, the expression of the stress tensor [Eq. (2)], together with the Fourier expansions [Eq. (5)], lead to the following simple

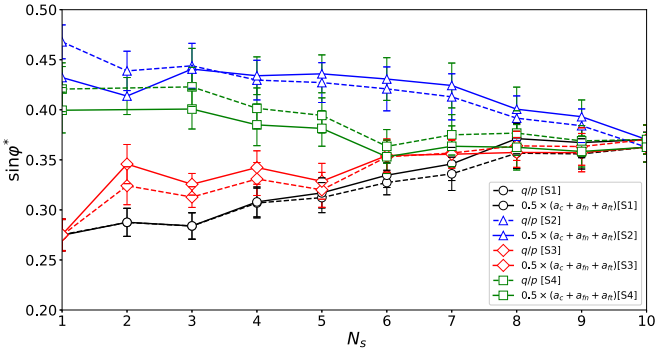

FIG. 12. Macroscopic shear strength $\sin\varphi^*$ as a function of N_s for all series (symbols and solid line) calculated from the stress tensor (see also Fig. 3) and predicted by Eq. (6) (dashed line).

approximation for the macroscopic friction [49,71]:

$$\sin\varphi^* \simeq \tfrac{1}{2}(a_c + a_{fn} + a_{ft}), \quad (6)$$

where the cross product between anisotropies have been neglected. Thus, Eq. (6) reveals the crucial role of these structural anisotropies in the understanding of the micromechanical origins of the macroscopic friction, in particular with respect of granular composition. The macroscopic friction angle $\sin\varphi^*$ predicted by Eq. (6) is shown in Fig. 12 as a function of N_s, for each series, together with those given by direct measurement [Fig. 3(a)].

The evolution of the contact and force anisotropies with N_s, and for each series, is shown in Figs. 13 and 14, respectively. We see that, in $S1$, the three anisotropies increase with N_s, underlying the observed increase in the macroscopic friction. In contrast, in $S2$ both a_c and a_{fn} initially grow from its value for $N_s = 1$, up to a maximum of $\simeq 0.35$ at $N_s = 7$ for a_c and $N_s = 3$ for a_{fn}, respectively, and then both decline at higher values of N_s. Then, we note that $a_c + a_{fn}$ is nearly constant with $N_s > 3$. The decrease in the macroscopic friction results thus from only the reduction of a_{ft}. For $S3$, the small increase of a_c and a_{fn}, together with the nearly independence of a_{ft} with N_s, explains the increment of the macroscopic friction angle with N_s. Then, for $S4$, both a_{fn} and a_{ft} are nearly constant with N_s, so that the decrease in the macroscopic friction is due to the decrease of a_c.

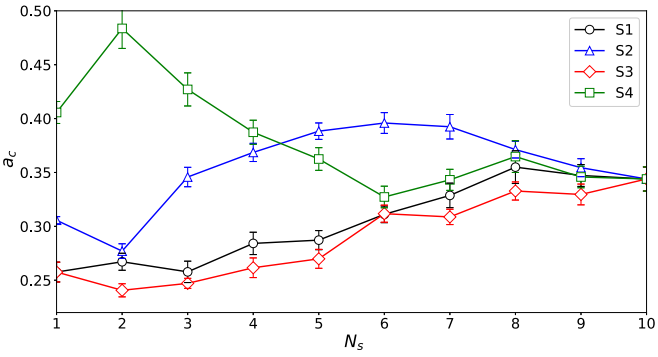

FIG. 13. Contact orientation anisotropies a_c as functions of N_s for all series.

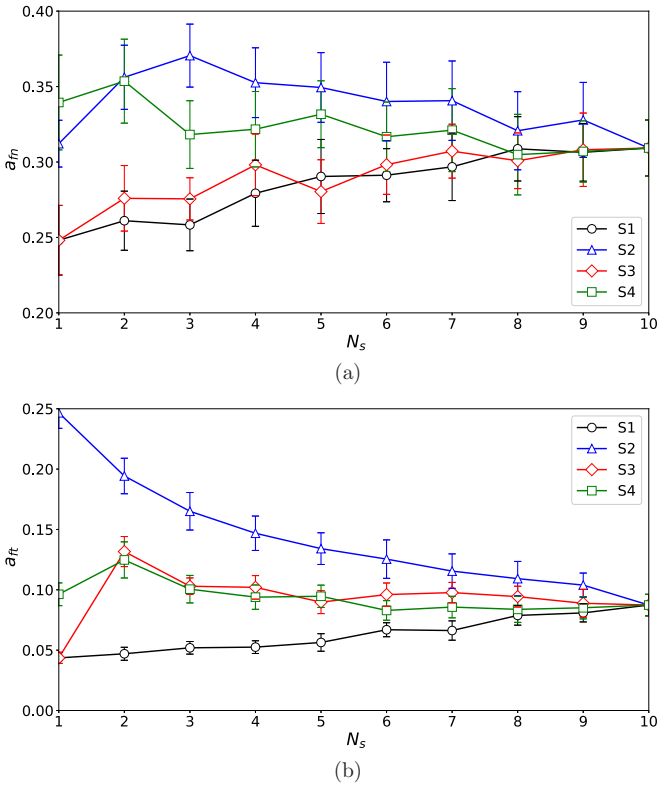

FIG. 14. Normal a_{fn} (a) and frictional a_{ft} (b) force anisotropies as functions of N_s for all series.

Physically, a_c describes the excess of the number of contacts oriented along the principal stress direction and their lack along the perpendicular direction. Therefore, we can expect a correlation between the contact anisotropy and the evolution of Z (see Fig. 6). We may deduce that adding more and more angular particles (the $S1$ case) let reorganize the ss-contacts along the vertical direction (Z is constant, whereas Z_{ss} increases with N_s). In contrast, adding more and more rounded particles (the $S2$ case) a loss of ss-contacts in the horizontal direction is induced (both Z and Z_{ss} decline with N_s). A similar mechanisms can be evoked for $S3$, since a_c increases whereas Z declines. In $S4$, we promote the reorganization of the contacts around each particle since a_c declines whereas Z is constant.

The normal force anisotropy a_{fn} reflects the larger value of the mean normal force at contacts oriented along the principal stress direction compared to those in the perpendicular direction. The increase of a_{fn} in $S1$ and $S3$ shows that stronger force chains are better transmitted along the principal stress direction at larger N_s values in these systems and, in effect, the mean normal force given by $\langle f_n \rangle = \int_0^\pi P(\theta)\langle f_n \rangle(\theta)d\theta$ increase as well. The frictional force anisotropy quantifies the stronger mobilization of friction forces at contacts oriented along $\theta_\sigma + \pi/4$ compared to those in the principal direction. The variation of a_{ft} in $S1$ and $S2$ is also compatible with the well-known proneness of facet particles to mobilize friction at side-side contacts [38,46], since the proportion of angular particles increases in $S1$ and declines in $S2$.

V. CONCLUSIONS, REMARKS, AND PERSPECTIVES

In summary, the effects of polydispersity by particle angularity on the mechanical behavior and microstructure of mixture granular materials were numerically investigated in the framework of the NSCD method. Several packings composed of 10000 particles under biaxial compression in rectangular box were systematically analyzed as a function of the number and the shape of the considered species. The number of species were varied from 1 to 10, and the shapes from disk to triangle. Three different cases were considered: (1) increase of angularity and species starting from disk, (2) decrease of angularity but increase of species starting from triangle and, (3) random angularity and increase of species starting from disk and from polygons.

It was shown that the mechanical behavior at the macroscale dependents on fine geometrical properties of the granular mixture. On the one hand, the shear strength increases if both the angularity and the proportion of each species in the sample increase. Otherwise, the strength drops. Unexpectedly, we also found that the shear strength varies monotonously with the number of species in random mixtures. On the other hand, the solid fraction varies conversely with the shear strength. Thus, packings may be looser although presenting a higher shear strength.

At the micro-scale, we analyzed in detail the particle connectivity and fabric and forces anisotropies. In the case $S1$, the increase of strength is due to a grow of the contact and normal force anisotropies. In the case $S2$, the decline of strength is a consequence of the drop in frictional anisotropy. For S3 and S4, i.e., for random mixtures, the variations of these anisotropies mutually compensate, which explain the monotonous variations as the number of species increases. This behavior is explained by the capability of angular particles to mobilize friction and better connect with neighboring particles.

This work represents a first step for a better understanding of the effects of particle shape polydispersity in granular materials by showing how the shear strength is affected by the dispersion of particle shapes. We see here that the definition of a "good" mixture that leads to "better" rheological properties is not evident. An initial answer would be, depending on feasibility, either to reduce the number of species in order to keep the most angular particles or to add more and more angular particles. In the objective of modeling realistic granular materials, further efforts are still necessary. They should take into consideration, for instance, more complex mixtures containing different particle forms such as elongated and/or non convex shapes both in two and three dimensions. In the same way, since friction mobilization plays a major role at large angularity, it would be interesting to investigate the effect of polydispersity by particle friction and combine effect of friction and particle angularity.

ACKNOWLEDGMENTS

We specially thank David Cantor for fruitful discussions. This work was supported by Royal Golden Jubilee Ph.D Program (Grant No. PHD/0062/2558) under Thailand Research Fund (TRF) and French Embassy in Thailand.

[1] L. T. Fan, J. R. Too, R. M. Rubison, and F. S. Lai, Powder Technology **24**, 73 (1979).
[2] J.-C. Géminard and W. Losert, Phys. Rev. E **65**, 041301 (2002).
[3] J.-S. Lee, M. Guimaraes, and J. C. Santamarina, J. Geotech. Geoenviron. Eng. **133**, 1136 (2007).
[4] D. K. Basson, S. Berres, and R. Bürger, Appl. Math. Modell. **33**, 1815 (2009).
[5] A. Džiugys and R. Navakas, Granular Matter **11**, 403 (2009).
[6] L. Vallejo and S. Lobo-Guerrero, Int. J. Geotech. Eng. **6**, 371 (2012).
[7] C. Lee, H. Shin, and J.-S. Lee, Int. J. Numer. Anal. Methods Geomech. **38**, 1651 (2014).
[8] J. Lee, T. Yun, and S.-U. Choi, Materials **8**, 3975 (2015).
[9] W. B. Fuller and S. E. Thompson, Trans. Am. Soc. Civ. Eng. **59**, 67 (1907).
[10] A. Amirjanov, Comput. Concr. **2**, 411 (2005).
[11] A. B. Yu and N. Standish, Powder Technol. **76**, 113 (1993).
[12] H. Brouwers and H. Radix, Cem. Concr. Res. **35**, 2116 (2005).
[13] B. Shekunov, P. Chattopadhyay, H. Tong, and A. Chow, Pharm. Res. **24**, 203 (2007).
[14] M. Wackenhut, S. McNamara, and H. Herrmann, Eur. Phys. J. E **17**, 237 (2005).
[15] P. Sollich and N. B. Wilding, Phys. Rev. Lett. **104**, 118302 (2010).
[16] M. R. Shaebani, M. Madadi, S. Luding, and D. E. Wolf, Phys. Rev. E **85**, 011301 (2012).
[17] V. Ogarko and S. Luding, Soft Matter **9**, 9530 (2013).
[18] L. Staron and J. C. Phillips, Phys. Rev. E **92**, 022210 (2015).
[19] L. Staron and J.-C. Phillips, Computat. Part. Mech. **3**, 367 (2016).
[20] L. Jing, C. Y. Kwok, and Y. F. Leung, Phys. Rev. Lett. **118**, 118001 (2017).
[21] C. Voivret, F. Radjaï, J.-Y. Delenne, and M. S. El Youssoufi, Phys. Rev. Lett. **102**, 178001 (2009).
[22] D.-H. Nguyen, E. Azéma, P. Sornay, and F. Radjaï, Phys. Rev. E **91**, 032203 (2015).
[23] N. Estrada, Phys. Rev. E **94**, 062903 (2016).
[24] E. Azéma, S. Linero, N. Estrada, and A. Lizcano, Phys. Rev. E **96**, 022902 (2017).
[25] J. Wiacek and M. Molenda, Int. J. Solids Struct. **51**, 4189 (2014).
[26] J. Wiącek and M. Molenda, Granular Matter **20**, 17 (2018).10.1007/s10035-018-0788-z
[27] K. Shinohara, M. Oida, and B. Golman, Powder Technol. **107**, 131 (2000).
[28] C. Nouguier-Lehon, B. Cambou, and E. Vincens, Int. J. Numer. Anal. Methods Geomech. **27**, 1207 (2003).
[29] G.-C. Cho, J. Dodds, and J. C. Santamarina, J. Geotech. Geoenviron. Eng. **132**, 591 (2006).
[30] N. Vandewalle, G. Lumay, O. Gerasimov, and F. Ludewig, Eur. Phys. J. E **22**, 241 (2007).
[31] P. W. Cleary, Powder Technol. **179**, 144 (2008).
[32] X. Garcia, L. T. Akanji, M. J. Blunt, S. K. Matthai, and J. P. Latham, Phys. Rev. E **80**, 021304 (2009).
[33] R. C. Hidalgo, I. Zuriguel, D. Maza, and I. Pagonabarraga, Phys. Rev. Lett. **103**, 118001 (2009).
[34] J. Baker and A. Kudrolli, Phys. Rev. E **82**, 061304 (2010).
[35] E. Azéma, F. Radjaï, and J.-N. Roux, Phys. Rev. E **91**, 010202(R) (2015).
[36] S. A. Galindo-Torres and D. M. Pedroso, Phys. Rev. E **81**, 061303 (2010).
[37] S. Abedi and A. A. Mirghasemi, Particuology **9**, 387 (2011).
[38] T. Kanzaki, M. Acevedo, I. Zuriguel, I. Pagonabarraga, D. Maza, and R. C. Hidalgo, Eur. Phys. J. E **34**, 133 (2011).
[39] T. Börzsönyi, B. Szabó, S. Wegner, K. Harth, J. Török, E. Somfai, T. Bien, and R. Stannarius, Phys. Rev. E **86**, 051304 (2012).
[40] K. Szarf, G. Combe, and P. Villard, Powder Technol. **208**, 279 (2011).
[41] CEGEO, B. Saint-Cyr, K. Szarf, C. Voivret, E. Azéma, V. Richefeu, J.-Y. Delenne, G. Combe, C. Nouguier-Lehon, P. Villard *et al.*, Europhys. Lett. **98**, 44008 (2012).
[42] H. Shin and J. C. Santamarina, J. Geotech. Geoenviron. Eng. **139**, 353 (2013).
[43] T. Börzsönyi and R. Stannarius, Soft Matter **9**, 7401 (2013).
[44] N. Stark, A. E. Hay, R. Cheel, and C. B. Lake, Earth Surf. Dyn. **2**, 469 (2014).
[45] E. Azéma, N. Estrada, and F. Radjaï, Phys. Rev. E **86**, 041301 (2012).
[46] E. Azéma, F. Radjaï, and F. Dubois, Phys. Rev. E **87**, 062203 (2013).
[47] B. Saint-Cyr, J.-Y. Delenne, C. Voivret, F. Radjaï, and P. Sornay, Phys. Rev. E **84**, 041302 (2011).
[48] E. Azéma, F. Radjaï, B. Saint-Cyr, J.-Y. Delenne, and P. Sornay, Phys. Rev. E **87**, 052205 (2013).
[49] E. Azéma and F. Radjaï, Phys. Rev. E **81**, 051304 (2010).
[50] M. Boton, E. Azéma, N. Estrada, F. Radjaï, and A. Lizcano, Phys. Rev. E **87**, 032206 (2013).
[51] S. Edwards and C. Mounfield, Physica A **210**, 290 (1994).
[52] C. R. Abreu, F. W. Tavares, and M. Castier, Powder Technol. **134**, 167 (2003).
[53] C. R. K. Windows-Yule, B. J. Scheper, W. K. den Otter, D. J. Parker, and A. R. Thornton, Phys. Rev. E **93**, 020901(R) (2016).
[54] T.-T. Ng, W. Zhou, G. Ma, and X.-L. Chang, Int. J. Solids Struct. **135**, 74 (2018).
[55] S. J. Roskilly, E. A. Colbourn, O. Alli, D. Williams, K. A. Paul, E. H. Welfare, and P. A. Trusty, Powder Technol. **203**, 211 (2010).
[56] X.-D. Ma and Y.-B. Zhang, Granular Matter **18**, 8 (2016).
[57] G.-G. Pereira and P. W. Cleary, Granular Matter **19**, 23 (2017).
[58] E. Azéma, I. Preechawuttipong, and F. Radjaï, Phys. Rev. E **94**, 042901 (2016).
[59] M. Jean, Comput. Meth. Appl. Mech. Eng. **177**, 235 (1999).
[60] F. Radjaï and F. Dubois, *Discrete-Element Modeling of Granular Materials* (Wiley-ISTE, New York, 2011).
[61] M. Renouf, F. Dubois, and P. Alart, J. Comput. Appl. Math. **168**, 375 (2004).
[62] V. Visseq, A. Martin, D. Iceta, E. Azéma, D. Dureisseix, and P. Alart, Computat. Mech. **49**, 709 (2012).
[63] C. Voivret, F. Radjaï, J.-Y. Delenne, and M. S. El Youssoufi, Phys. Rev. E **76**, 021301 (2007).
[64] GDR MiDi, Eur. Phys. J. E **14**, 341 (2004).
[65] J. J. Moreau, Eur. J. Mech. A, Solids **13**, 93 (1994).
[66] L. Staron, F. Radjaï, and J.-P. Vilotte, Eur. Phys. J. E **18**, 311 (2005).

[67] J.-J. Moreau, in *Friction, Arching, Contact Dynamics,* edited by D.-E. Wold and P. Grassberger (World Scientific, Singapore, 1997), pp. 232–247.

[68] J.-K. Mitchell and K. Soga, *Fundamentals of Soil Behavior* (Wiley, New York, 2005).

[69] H. Troadec, F. Radjaï, S. Roux, and J. C. Charmet, Phys. Rev. E **66**, 041305 (2002).

[70] M. Acevedo, R. C. Hidalgo, I. Zuriguel, D. Maza, and I. Pagonabarraga, Phys. Rev. E **87**, 012202 (2013).

[71] L. Rothenburg and Bathurst, Geotechnique **39**, 601 (1989).